



Original Research

The role of inflammation in driving left ventricular remodeling in a pre-HFpEF model

Maria L Loredó-Mendoza^{1,2} , Israel Ramirez-Sanchez^{1,3},
Moises Muratt Bustamante-Pozo^{1,3}, Marcos Ayala¹, Viridiana Navarrete¹,
Alejandra Garate-Carrillo^{1,3} , Bruce R Ito³, Guillermo Ceballos¹, Jeffrey Omens³ and
Francisco Villarreal^{3,4}

¹Seccion de Estudios de Posgrado e Investigacion, Escuela Superior de Medicina, Instituto Politecnico Nacional, Mexico 07738, Mexico;

²Department of Histopathology, School of Medicine, Universidad Panamericana, Ciudad de Mexico 03920, Mexico; ³Department of Medicine, School of Medicine, University of California, San Diego, CA 92093-0021, USA; ⁴VA San Diego Healthcare, San Diego, CA 92161, USA

Corresponding author: Francisco Villarreal. Email: fvillar@ucsd.edu

Impact statement

The incidence of HFpEF continues to increase and ~2/3 of the patient population are post-menopausal women. Unfortunately, most studies focus on the use of male animal models of remodeling. In this study, however, using female rats to set a model of pre-HFpEF, we provide insights to possible mechanisms that contribute to HFpEF development in humans that will lead us to a better understanding of the underlying pathophysiology of HFpEF.

Abstract

We previously reported on the development of left ventricular (LV) structural and functional changes in an aged, female rat model where the effects of ovariectomy and excess weight (stimulated by fructose in water) were also explored. Ovariectomy and/or excess weight led to a prolongation of active relaxation, loss of cardiac output, and LV fibrosis in the setting of preserved ejection fraction. In this follow-up study, we wished to characterize the possible role of LV inflammation, oxidative stress (OS), and cell death in inducing such changes. Four experimental groups were studied: young (3 months old), aged (18 months old), aged + ovariectomy (OVX), and aged + ovariectomy + 10% fructose (OVF). Using conventional histology and immunohistochemistry of myocardium as well as biochemical assays of

plasma samples, we document the presence of inflammatory cell aggregates in LV myocardium which are associated to high levels of plasma inflammatory cytokines (IL-1 β , TNF- α , IFN- γ , TGF- β 1) and OS (carbonyl proteins) in aged, OVX, and OVF vs. young animals. In the inflammatory areas, normal cardiac tissue was substituted by replacement and interstitial fibrosis and M1 macrophages, (as per by CD68 immunostaining) as we all as by co-localization with TGF- β 1. We also document increases in plasma troponin I levels, loss of capillary density, cardiomyocyte hypertrophy, and death. Select changes were further aggravated by ovariectomy and/or excess weight. In conclusion, aging in the female rat heart, when compounded with estrogen depletion and excess weight promotes the development of greater levels inflammation, OS, fibrosis, capillary rarefaction, cardiomyocyte hypertrophy, and injury/death. These factors likely play an important role in the development of LV remodeling that leads to the development of a “pre-HFpEF” phenotype.

Keywords: Myocardial macrophages, cardiomyocyte degeneration, cardiomyocyte necrosis, estrogen deprivation, inflammatory biomarkers

Experimental Biology and Medicine 2020; 245: 748–757. DOI: 10.1177/1535370220912699

Introduction

Heart failure (HF) is the most common cause for hospitalization in older patients and represents the greatest Medicare cost in the US.^{1,2} Up to 50% of HF patients are now recognized to have what is termed HF with preserved

ejection fraction or HFpEF. HFpEF is a poorly understood disease with no effective therapies.^{3,4} In HFpEF patients, the preservation of left ventricular (LV) morphology and ejection fraction (while at rest) in the setting of diastolic dysfunction are recognized as common features.⁴

The insufficient delivery of cardiac output (CO) arises during increased demand where the LV fails to accommodate greater filling volumes. To better understand its pathophysiological underpinnings and explore potential novel therapies, animal models of pre-HFpEF are needed. HFpEF is most common in elderly, post-menopausal female patients (2:1 vs. men).² In women, the disease is frequently associated with the presence of hypertension as well as excess weight/obesity.⁵

While the biological processes related to the development of HFpEF are poorly understood, inflammation is recognized as a prominent suspect. We previously reported on the development of LV structural and functional changes in an aged, female rat model where the effects of ovariectomy and excess weight were also explored us.⁶ Ovariectomy and/or excess weight led to a prolongation of LV relaxation, a loss of CO as well as LV and papillary muscle fibrosis in the setting of preserved EF. On the basis of these findings, we termed this aged, female rat model as “pre-HFpEF”. The aim of the present study was to examine in this model of pre-HFpEF the role that oxidative stress (OS), inflammation, and cell death may play in the development of morphological and fine structural changes, which could determine the functional, macro-, and microscopic heart derangements previously reported by us.

Methods

Study design

Three-month-old (young) and 18-month-old (aged) female Fischer 344 rats were used. Animals were obtained from the National Institutes of Health (NIH)/National Institutes of Aging breeding colony. The NIH Guide for Care and Use of Laboratory Animals was followed, and the Institutional Animal Care and Use Committee of the University of California San Diego approved the protocol. Animals were housed two per cage with 12-h light-dark cycles. Animal diet included regular rat chow and water *ad libitum*. After a period of one week of conditioning, aged rats were randomly allocated into three groups: aged (n = 8), ovariectomy (OVX, n = 16), and ovariectomy + 10% fructose in drinking water (OVF, n = 16). Under isoflurane anesthesia, OVX and OVF groups underwent bilateral oophorectomy via dorsal incision.⁶ OVF animals started fructose-water intake one week after surgery and continued for three months. Young animals were used as controls. All animals were maintained under comparable conditions for three months (i.e. until the age of 21 months).

Heart processing

At the end of the *ex vivo* study, hearts were perfused through the aorta with ice-cold perfusion solution (0.05 M KCl and 0.015 M 2,3-butanedione monoxime) at a constant pressure (10 mmHg) for 5 min then perfusion and immersion fixed with 10% neutral phosphate buffered saline (PBS) buffered formalin.⁶ After a 24-h fixation period, hearts were weighed and trimmed before sectioning at the mid-ventricular region, obtaining one LV base ring

(#1) and one apical ring (#2) from each heart (Figure 1). Fixed rings were embedded in paraffin, then 5- μ m thick sections were obtained and mounted onto glass slides.

Conventional histology

To grossly evaluate the inflammatory infiltrate, four sections per LV (2 from ring #1 and 2 from ring #2) were stained with hematoxylin and eosin (HE). In Figure 2, whole ring of LV sections were stained. HE stained sections were evaluated at 100 \times , 200 \times , and 400 \times magnification with a Zeiss Axiophot 2 light microscope. Representative digital photomicrographs (10/section) of each individual ring were randomly acquired and analyzed for the presence of an inflammatory cell infiltrate. Low magnification images were used to quantify inflammatory cells in aggregates (nests) of >40 cells. Evaluation of HE stained slides was performed at 200 \times in order to initially analyze LV inflammatory cell infiltration and nest formation. A 400 \times was used to identify myocyte injury and characterize the possible identity of small inflammatory nests. Quantification was done in seven animals/group by a blind operator. Aggregates of inflammatory cells in association with necrotic or degenerated cardiomyocytes were duly noted. Picosirius red staining and associated levels of LV and papillary fibrosis were previously reported by us⁶ and used in this study to correlate to inflammation and cell death.

Immunofluorescence and immunohistochemistry

Immunolabeling was performed in LV sections after deparaffinization. For M1 macrophage identification, slides were incubated in 0.05% trypsin at pH 7.8 for 12 min at 37°C for antigen retrieval. Then incubated overnight at 4°C with anti-CD68 primary antibody (Abcam [ED1] ab31630) at 1:50 dilution, washed with PBS-Tween, and incubated for 60 min at room temperature (RT) with secondary antibody (Goat anti-mouse IgG H + L), FITC-conjugate (Invitrogen, Life Tech, Cat. No. A16079) 1:100 dilution. For nuclear staining propidium iodide was used. To evaluate LV

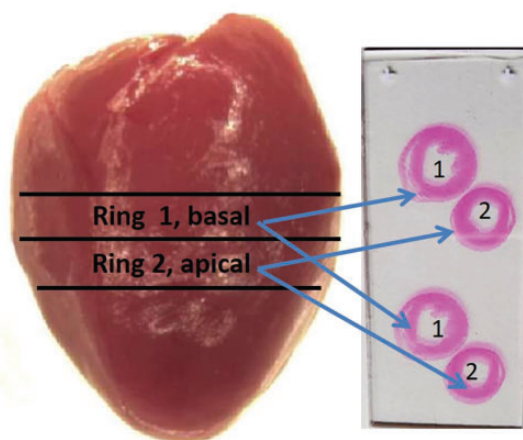


Figure 1. Heart processing. Image of a fixed rat heart with midventricular lines indicating where the cuts were done yielding two rings from each heart, one basal and one apical. From each ring, two sections were mounted onto a slide. (A color version of this figure is available in the online journal.)

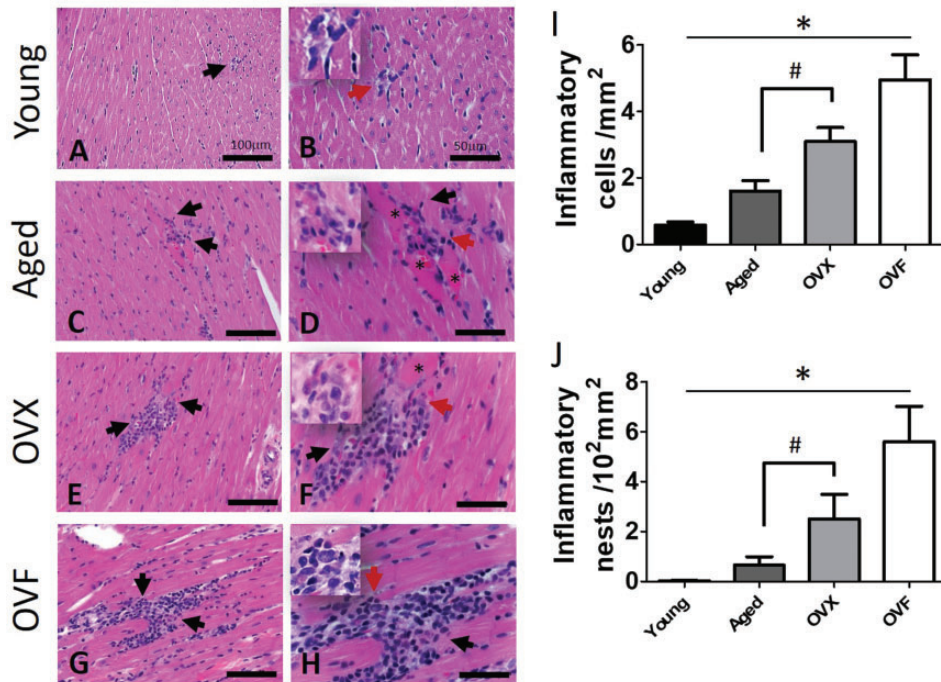


Figure 2. Inflammatory cell infiltration in left ventricle (LV). (a) Representative images of hematoxylin and eosin stained LV sections from each group, demonstrating areas of myocyte loss substituted by nests or aggregates of inflammatory cells (arrows) of increasing size from (a) to (g) (left panel 200 \times magnification, scale bar = 100 μ m). Right panel (400 \times , scale = 50 μ m) denotes the presence of degenerated and fragmented myocytes in vicinity of inflammatory aggregates. Note in aged (d) and OVX (f) the eosinophilic cytoplasm of degenerated myocytes (*), and in OVX (h) their fragmentation (arrow). Red arrows in left panel shows areas magnified in inserts. Inflammatory cells quantitation (i) in young, aged, OVX, and OVX. (j) Inflammatory nests (40+ cells) in the same groups. Values are mean \pm SEM, $n = 7-8$ animals/group, * $P < 0.001$ vs. young, # $P < 0.05$ vs. aged and vs. OVX by ANOVA. (A color version of this figure is available in the online journal.)

capillary density, antigen retrieval was achieved by a 40 min exposure of sections in a boiling bath to a 0.5M Tris base buffer at pH 10. Sections were immunolabeled with a mouse anti-CD31 antibody (Abcam CD31 [P2B1] ab24590), which labels endothelial cells and with anti-mouse secondary antibody FITC-conjugated (Invitrogen, Life Tech, Cat. No. A16079) 1:100 dilution. To enhance immunofluorescence, all sections were subsequently incubated with tyramide amplification System Plus Fluorescein (Perkin Elmer, NEL 741001KT) and with 1:100 antifluorescein-peroxidase conjugated antibody (Perkin Elmer, NEF71000) for 30 min, followed by the application of the FITC tyramide amplifier (1:100) during 5 min. For transforming growth factor (TGF)- β 1 immunolabeling, a boiled, citrate buffer at pH 6 was used for antigen retrieval. Slides were incubated overnight at 4 $^{\circ}$ C with 1:100 dilution of the primary antibody (Abcam ab25121) followed by incubation with HRP conjugated secondary antibody (Cell Signaling 7074) for 1 h at RT. Color development (brown) was generated using diaminobenzidine as a substrate. For the analysis of immunolabeling-based histology, 15 images were randomly obtained from each LV section at 200 \times or 400 \times magnification (5 animals/group). For the analysis of CD68 positive cells and TGF- β 1 immunolabeling, 10 images were obtained at 100 \times and 400 \times magnification, respectively. Capillaries were quantified manually by a blind operator, taking into account clear-lumen tubular structures positive for CD31 staining. The number of capillaries is expressed per mm 2 .

Myofiber cross-sectional area

To quantify myofiber (cardiomyocyte) cross-sectional area (CSA), sections were stained with wheat germ agglutinin-Alexa Fluor 633 conjugate (Invitrogen, W 21484). Using 400 \times magnification ($n = 5$ hearts/group), 15 digital photomicrographs from non-overlapping fields were taken. The cardiomyocyte mean CSA from around 450 cardiomyocytes was calculated using a semi-automatic computerized image analysis software (Axiovision Rel 4.8.2 Zeiss). CSA is expressed in μ m 2 .

TUNEL staining

To detect apoptotic cell death, LV sections were subjected to the DeadEndTM Fluorometric TUNEL System (Promega, G3250), according to manufacturer instructions. After labeling, for the quantification of apoptotic nuclei, slides (4 LV sections from each animal) were visualized at 200 \times magnification and positive TUNEL nuclei counted by a blind operator in a total of 12 images captured. The number of TUNEL stained nuclei is expressed per mm 2 .

Plasma measurements

At the end of the study and before harvesting the hearts, blood samples were collected from the right ventricle, transferred to a Ethylenediaminetetraacetic acid (EDTA)-coated vials and centrifuged at 252g for 10 min. Plasma was recovered and used for determination of troponin I (MyBioSource Cat# MBS727624) and TGF- β 1 (Invitrogen

Cat# 88-50680-22) by ELISA kits following manufacturer instructions. Absorbance as optical density (OD) of the samples was determined at a wavelength of 450 nm in a BioQuant spectrophotometer (BioTek, Inc.). Samples were evaluated in duplicate, and concentration values were obtained using a standard curve. For interleukin 1-beta (IL-1 β), tumor necrosis factor alpha (TNF- α), interferon gamma (INF- γ), and granulocyte-macrophage colony stimulator factor (GM-CSF) plasma samples were analyzed by the use of a Milliplex xMAP rat cytokine magnetic-bead Luminex system (Millipore EMD Cat# RecytMAG-65K) following manufacturer instructions. Plasma protein carbonylation content was used as an indirect indicator of OS, a recognized trigger of inflammation. Carbonyl protein levels were measured using a dinitrophenylhydrazine (DNPH)-based colorimetric assay kit (Cayman Chemical 10005020). Absorbance as OD in samples was measured in a μ Quant spectrophotometer (BioTek Instruments, Inc.) at a wavelength of 385 nm.

Statistical analysis

Data shown are presented as mean \pm standard error of the mean (SEM). Statistical analyses used one-way ANOVA with Tukey's post hoc test or Student's unpaired t-test (when appropriate) using GraphPadPrism version 5.02 (GraphPad Software, 2008, San Diego, CA, USA). Results were considered statistically significant at a value of $P < 0.05$.

Results

Table 1 summarizes the major cardiovascular endpoints recorded in rats using a Millar catheter.

The analysis of LV inflammatory cell infiltrate identifies increased cell aggregation in aged, OVX, and OVF groups vs. young (Figure 2(a) to (h)). The inflammatory infiltrate was distributed in cell aggregates or nests and it was mainly localized in deeper layers of myocardium. Cell aggregates ranged from small (\sim 5 cells) to very large ($>$ 80 cells) (Figure 2(c) to (h)). Cell aggregates appear surrounded by necrotic cardiomyocytes, degenerated tissue, or fibrotic areas. Injured muscle was identified by the absence of sarcomeric structures and by the strong affinity for eosin staining. Based on morphological and nuclear characteristics, most of the cell infiltrates were pre-

identified as macrophages. Fibro-inflammatory areas were also identified closer to the subendocardial region. The latter areas also included cells identified by shape as fibroblasts (Figure 2(e) to (h)) surrounded by collagen. Inflammatory cell numbers were greater in aged, OVX, and OVF groups vs. young ($P < 0.05$) (Figure 2(i)). Comparison of aged vs. OVX or OVF groups also showed increased number of inflammatory cells in OVX and OVF ($P < 0.05$) (Figure 2(i)). No differences were found between OVX vs. OVF. The amount of large inflammatory nests ($>$ 40 cells) was higher in aged, OVX, and OVF groups vs. young ($P < 0.05$) (Figure 2(j)). When comparing large nest from aged vs. OVX or OVF there was also a statistical difference ($P < 0.05$) (Figure 2(j)).

Figure 3 reports on the presence of CD68+ M1 macrophages. A large amount of CD68+ cells were detected in aged, OVX, and OVF (Figure 3(a)). In agreement, plasma levels of GM-CSF (Figure 3(b)) were increased in aged, OVX, and OVF vs. young ($P < 0.05$) and were higher in OVF vs. aged which parallels with CD68 immunolabeling. Representative images of LV section TUNEL+ nuclei are shown in Figure 4(a) demonstrating higher levels in aged, OVX, and OVF animals. As shown in Figure 4(b), the total number of TUNEL+ nuclei were significantly higher in aged, OVX, and OVF vs. young ($P < 0.001$). Plasma troponin I quantities (Figure 4(c)) demonstrate higher levels in aged, OVX, and OVF groups vs. young ($P < 0.001$).

The subendocardium and papillary muscles deserved special attention as fibrotic tissue was highly concentrated in such areas.⁶ The inflammatory cell infiltrate (by HE staining) in subendocardium appeared highly concentrated in aged, OVX, and in particular, OVF animals (Figure 5(b) to (d)) as compared to young animals (Figure 5(a)). Major fibro-inflammatory areas in papillary muscles were also detected in sections of aged, OVX, and OVF animals (Figure 5(k) and Figure 5(l)) with no changes in young animals (Figure 5(i)). Localized fibrosis appeared mostly interstitial in subendocardium of aged rats and reparative (patch-like) in OVX and OVF groups (Figure 5(f) to (h)). In papillary muscles of aged group, discrete foci of reparative fibrosis and less inflammatory cells were observed (Figure 5(n)), while papillary muscles OVX (Figure 5(o)) and OVF (Figure 5(p)) groups exhibited greater areas of localized replacement fibrosis. The subendocardium and

Table 1. Major cardiovascular parameters recorded using a Millar catheter of young (Y), aged (A), ovariectomized (OVX), and ovariectomized + fructose (OVF) Fischer 344 female rats.

	Y (n = 8)	A (n = 8)	OVX (n = 16)	OVF (n = 16)	ANOVA P
Body weight (g)	178.0 \pm 2.1	238.3 \pm 8.6 [#]	253.4 \pm 5.4 [#]	290.8 \pm 4.9 ^{#,*}	<0.001
Heart rate	339.0 \pm 7.1	302.2 \pm 11.3	271.4 \pm 11.3 [#]	287.9 \pm 9.9 [#]	0.002
Aortic diastolic pressure (mmHg)	99.9 \pm 3.3	115.3 \pm 5.6	112.2 \pm 3.8	111.6 \pm 3.8	0.318
Aortic systolic pressure	122.1 \pm 6.9	180.5 \pm 9.2 [#]	163.6 \pm 7.4 [#]	166.7 \pm 11.6 [#]	0.009
Mean aortic pressure	110.4 \pm 4.1	142.7 \pm 7.4	134.1 \pm 5.0	134.1 \pm 5.0	0.051
Tau (s)	10.0 \pm 0.3	12.6 \pm 0.9 [#]	13.8 \pm 0.4 [#]	13.4 \pm 0.5 [#]	<0.001
Ejection fraction (%)	55.1 \pm 4.1	61.4 \pm 7.0	53.2 \pm 2.6	56.3 \pm 5.7	0.747
Cardiac index (ml/min/m ²)	0.212 \pm 0.010	0.169 \pm 0.017 [#]	0.114 \pm 0.006 ^{#,*}	0.108 \pm 0.007 ^{#,*}	<0.001

Values are mean \pm SEM. NA: subgroup analysis not applicable. Cardiac index normalized to estimated body surface area. [#] $P < 0.05$ vs. young, ^{*} $P < 0.05$ vs. aging. Data retrieved from Bustamante et al.⁶

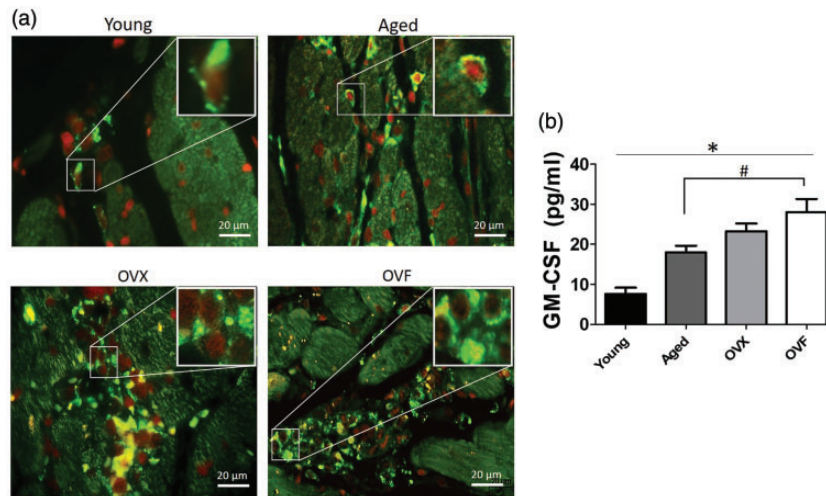


Figure 3. Presence of CD68⁺ M1 macrophages in left ventricle (LV) and granulocyte-macrophage-colony stimulating factor (GM-CSF) plasma levels. (a) Images of CD68⁺ cells in green (FITC in cytoplasm and nuclei stained in red with propidium iodide) in inflammatory infiltrates, locate magnified areas in squared inserts. Young animals show very few CD68⁺ cells in myocardium. Aged animals depict polygonal and spindle-shaped M1 macrophages, isolated or in small aggregates. OVX and OVF groups show many rounded and oval-shaped M1 macrophages constituting a large nest, some of the macrophages have yellow autofluorescent debris in their cytoplasm (400 \times magnification, scale bar = 20 μ m). (b) GM-CSF plasma levels in young, aged, OVX, and OVF rats. Values are mean \pm SEM, $n = 7$ –8/group, * $P < 0.001$ vs. young, # $P < 0.05$ vs. aged by ANOVA. (A color version of this figure is available in the online journal.)

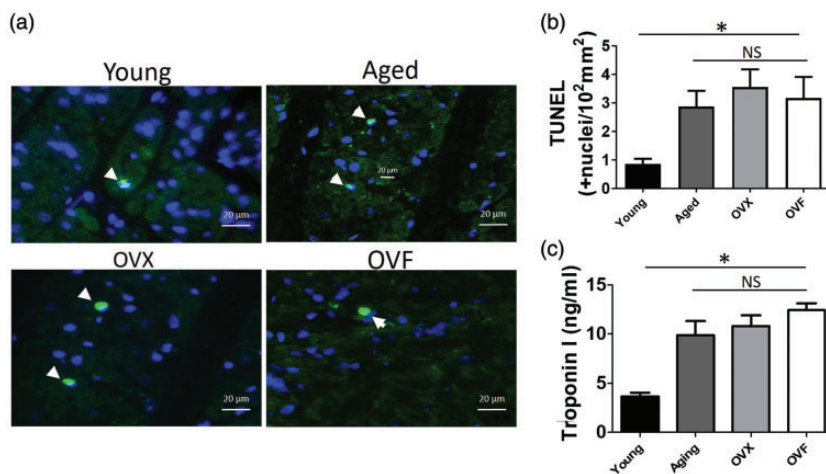


Figure 4. TUNEL staining of left ventricle (LV) and plasma troponin I levels. (a) Representative images of TUNEL⁺ cardiomyocyte nuclei in light green (arrows). Image is merged with the blue DAPI staining for nuclei. (b) Bar graph of TUNEL⁺ nuclei in young, aged, OVX, and OVF rats. Values are mean \pm SEM $n = 7$ –8 animals/group of four sections/heart (magnification 400 \times , scale bar = 20 μ m), * $P < 0.0001$ vs. young by ANOVA. (c) Plasma troponin I levels in the same groups. (A color version of this figure is available in the online journal.)

papillary muscles of young rats showed no major structural alterations (Figure 5(m)).

Analysis of protein carbonylation demonstrated higher levels in aged (60.3 nmol/ml \pm 10 SEM with a P value < 0.05), OVX (74.8 nmol/ml \pm 12.1 SEM $P < 0.01$), and OVF (94.5 nmol/ml \pm 9.3 SEM $P < 0.001$) vs. young (25.9 nmol/ml \pm 9.3 SEM). Results from plasma levels of IL-1 β , TNF- α , and IFN- γ are shown in Figure 6(a) to (c). Higher levels of all cytokines were detected in aged, OVX, and OVF groups vs. young ($P < 0.001$). TNF- α and IFN- γ showed higher levels in OVX and OVF groups vs. aged ($P < 0.05$). Plasma TGF- β 1 levels were higher in aged, OVX, and OVF vs. young ($P < 0.001$) (Figure 7(a)). Also, aged vs. OVF were different ($P < 0.05$). A similar pattern of gradual increases was observed in myocardial tissue sections by immunohistochemistry, where TGF- β 1 was

increased in aged, OVX, and OVF vs. young (Figure 7(b)). As shown in Figure 8(a) and (b), significantly higher cardiomyocyte CSA was observed in aged, OVX, and OVF groups vs. young group ($P < 0.001$). The OVF group was higher vs. aged ($P < 0.001$) as shown in Figure 9(a) and (b). Capillary density (Figure 9(a)) results were expressed as the number of endothelial tubular structures per mm² positive for CD31 (Figure 9(b)). Capillary density was significantly decreased in aged, OVX, and OVF groups vs. young ($P < 0.0001$). OVF animals evidenced greater decreases ($P < 0.05$) vs. aged.

Discussion

Using a female rat model of pre-HFpEF, we explored the roles that OS, inflammation, and cell death may play in the

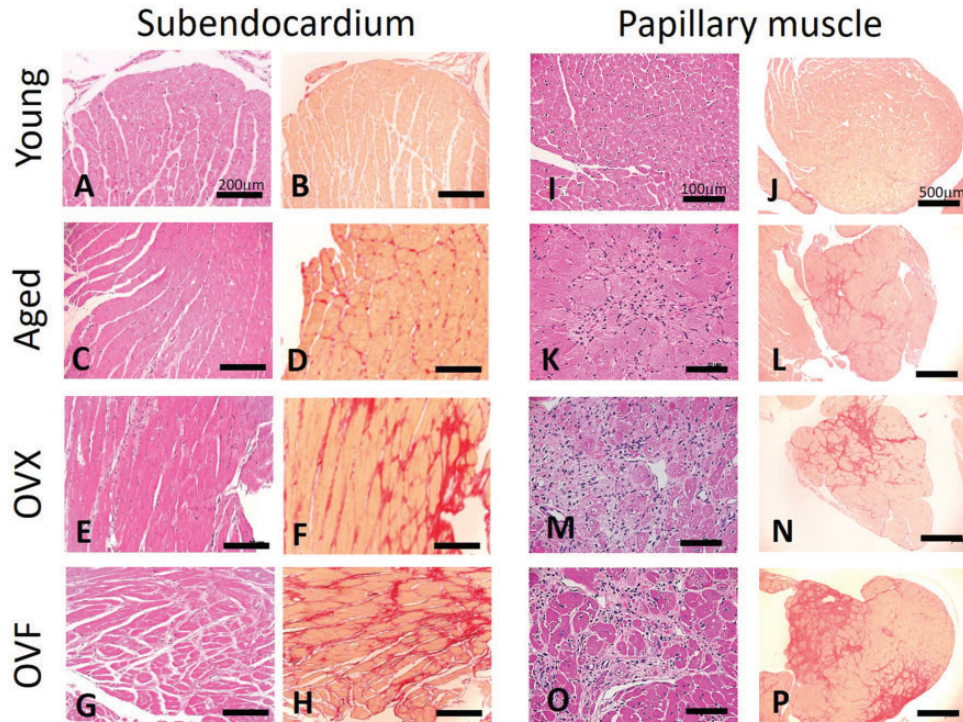


Figure 5. Representative images of left ventricular subendocardium (100 \times magnification) and papillary muscle. Hematoxylin and eosin (HE, left panels) and Picrosirius red for collagen staining (right). HE images of subendocardium from young (a) animals without major alterations and (b) no fibrosis. Aged LV demonstrating modest inflammatory cell infiltrates (c,d) mild interstitial fibrosis. OVX and OVF LV illustrates higher number of inflammatory cells (e,g), and interstitial and replacement type fibrosis (f,h). Papillary muscle HE (200 \times magnification) and Sirius red stained sections (50 \times magnification), demonstrating no changes in the young group (i,j); the aged animals depict a clear fibro-inflammatory area (k,l), OVX (m,n) and OVF (o,p) animals show larger similar areas with higher number of inflammatory cells. (A color version of this figure is available in the online journal.)

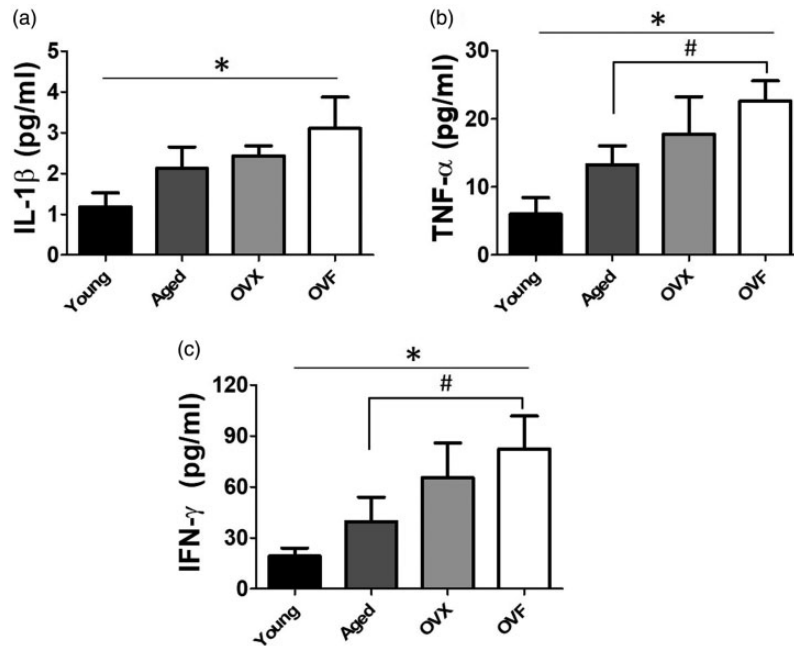


Figure 6. Proinflammatory cytokines levels in plasma. Quantification of IL-1 β (a), TNF- α (b), and IFN- γ (c) plasma levels in young, aged, OVX, and OVF animals. Values are mean \pm SEM, $n = 7-8$ animals/group, * $P < 0.001$ vs. young, # $P < 0.05$ vs. aged by ANOVA.

development of structural and functional changes previously reported by us. On the basis of histological results, aging appears sufficient to trigger the development of inflammation that co-localized with areas of fibrosis and

increased TGF- β 1 staining mainly, in deeper layers of the heart, which was in general, further aggravated by the absence of ovarian hormones and excess weight. Cardiomyocyte hypertrophy was detected as well as

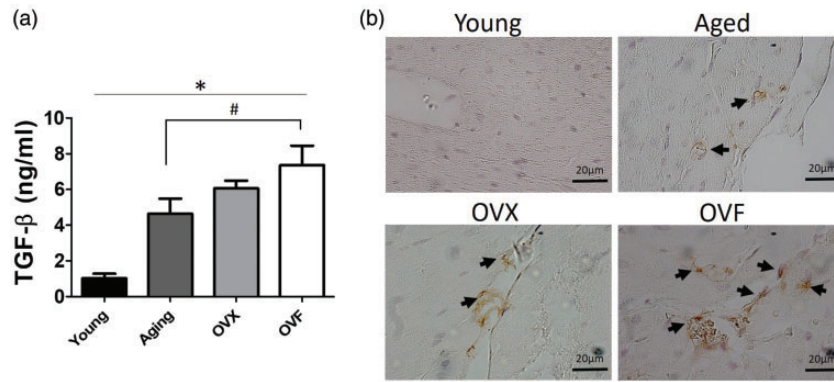


Figure 7. TGF- β immunohistochemistry in left ventricle (LV) and TGF- β plasma. (a) Representative images (400 \times magnification) of LV sections stained for TGF- β demonstrating no positive labeling in young and positive (brown) in non-myocyte cells in aged, OVX, and OVX animals. (b) Plasma TGF- β levels in the same groups. Values are mean \pm SEM, $n = 7-8$ animals/group, * $P < 0.001$ vs. young, # $P < 0.05$ vs. aged by ANOVA. (A color version of this figure is available in the online journal.)

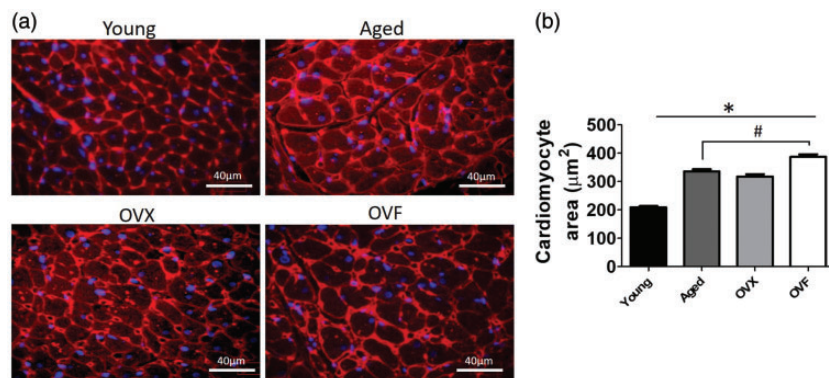


Figure 8. Left ventricular (LV) cardiomyocyte size measurements. (a) Representative images of LV myocardium cross-section (400 \times magnification). Cardiomyocyte membrane stained with wheat germ agglutinin in red and nuclei in blue. (b) Bar graph of cross-sectional area in young, aged, OVX, and OVX rats. Values are mean \pm SEM, $n = 7-8$ animals/group, * $P < 0.001$ vs. young by ANOVA, and # $P < 0.05$ vs. aged by unpaired t-test. (A color version of this figure is available in the online journal.)

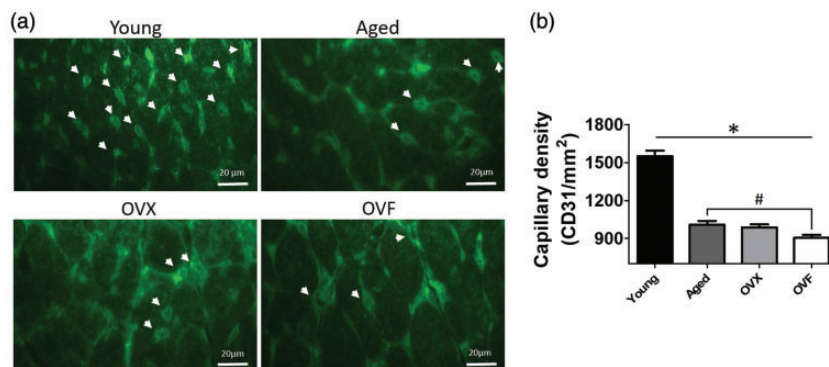


Figure 9. Left ventricular (LV) capillary density measurements. (a) Representative images of LV sections immunolabeled with CD31-FITC in green (63 \times magnification) which demonstrate capillaries. Note the abundance of capillarity in young LV relative to the other groups. (b) Bar graph of capillary density in young, aged, OVX, and OVX rats. Values are mean \pm SEM, $n = 7-8$ animals/group, * $P < 0.001$ vs. young by ANOVA, and # $P < 0.05$ vs. aged by unpaired t-test. (A color version of this figure is available in the online journal.)

capillary rarefaction. Localized areas of myocyte necrosis and/or apoptosis were also evident. In blood, there was evidence for OS as well as muscle damage, which occurred in the setting of increases in pro-inflammatory cytokines.

There are three major types of myocardial fibrosis. One is replacement fibrosis which substitutes for areas of myocyte death. Interstitial fibrosis is defined as increases in

collagen surrounding myocytes and finally, perivascular fibrosis which arises around blood vessels. In humans, there is evidence for increased levels of myocardial fibrosis in the setting of normal aging, which can be further aggravated by diseases such as atrial fibrillation and HF.⁷⁻⁹ It is believed that myocardial fibrosis increases chamber stiffness leading to a loss in diastolic function. While diastolic

dysfunction is not universally present with HFpEF, it is believed that myocardial fibrosis is a key contributor to the inability of the LV to accommodate higher filling volumes in a large percentage of patients.⁸ In rodents, multiple studies have reported increased levels of cardiac collagens/fibrosis with aging. However, the great majority of studies rely on male animals. A review article by Biernacka and Frangogiannis, provides a comprehensive summary of reports in animals.¹⁰ Eghbali *et al.*, demonstrated that collagen content in the LV increased from 5.5% of total protein in young Fischer 344 rats to ~12% in old animals.¹¹ Collagen content is also significantly increased in old rabbits¹² and mice.¹³ The relative proportion of types I and III collagen can change with time. With aging, Mays *et al.* reported on increases in type III collagen in myocardium of Lewis rats.¹⁴ Studies in animals also provide strong evidence for aging associated increases in cardiomyocyte hypertrophy, damage, and fibrosis. In normal aged hearts, there is progressive myocyte necrosis and apoptosis.¹⁵ As myocytes have a limited capacity to divide, surviving cells develop compensatory hypertrophy that is accompanied by replacement fibrosis.¹⁶ Aged rodent models of hypertension typically display enhanced levels of all three types of fibrosis.¹⁰

Multiple studies have reported on age-dependent loss of mitochondrial function that links to increased reactive oxygen species production.¹⁰ As myocardium has the highest density of mitochondria, it is also highly vulnerable to reactive oxygen species damage leading to cardiomyocyte death. High OS levels may also be secondary to a loss in the capacity to buffer reactive oxygen species. We recently reported that in the aging male mouse heart, well-recognized factors (e.g. sirtuin 1) that regulate mitochondrial biogenesis and mitochondrial structure and/or function-related endpoints (e.g. mitofilin and citrate synthase) were significantly reduced vs. young.¹⁷ With aging, high levels of myocardial protein carbonylation were detected and were associated with depressed levels of reactive oxygen species buffering system components including superoxide dismutase, catalase, glutathione peroxidase, and thioredoxin. Decreases occurred in the presence of reduced levels for the sirtuin 1, 3, and Nrf2, which are known to positively regulate mitochondrial biogenesis and reactive oxygen species buffering systems.

High levels of reactive oxygen species and associated tissue damage triggers an inflammatory response, which importantly contributes to tissue remodeling and fibrosis.⁹ Although most inflammatory cells have demonstrated to play important roles in myocardial remodeling, monocytes/macrophages appear key as per their ability to orchestrate a concerted set of events that can lead to tissue remodeling, repair (e.g. as per phagocytosis of dead cells), fibrosis, and angiogenesis. Macrophages can be described as displaying two prominent "opposing" polarities.⁹ Activated (i.e. pro-inflammatory) types are described as M1 and can be induced by cytokines such as GM-CSF, TNF- α , IL-1 β , and IFN- γ . M1 macrophages can produce pro-inflammatory and pro-fibrotic cytokines such as TGF- β 1 and fibroblast growth factors. In contrast, M2 macrophages express high levels of IL-10 and associate

with the resolution of inflammation and tissue repair. Of the pro-fibrotic cytokines, TGF- β 1 appears central to the development of fibrosis. Multiple studies have demonstrated the upregulation of TGF- β 1 in animal models of adverse remodeling/fibrosis and in fibrotic human hearts.^{9,10,18} The use of transgenic models of altered expression of TGF- β 1 and associated receptors have also corroborated its central role in the development of fibrosis.⁹ Of interest is that aging-associated increases in pro-inflammatory and pro-fibrogenic cytokines are also reported to occur systemically as per their high blood levels leading to the use of the term inflamm-aging which is suspected to contribute to the development of tissue remodeling in other organs.¹⁹

With aging, capillary density has been reported in animals as decreased in tissues such as brain.²⁰ Myocardial capillary rarefaction has been reported in HFpEF patients.⁸ It is believed that capillary rarefaction arises from aging associated-induced endothelial dysfunction secondary to reactive oxygen species-induced damage and inflammatory processes.²⁰ Altogether, the results provided in this study as per aging alone, align with those previously reported for male rodent models of aging where there is evidence for cardiomyocyte death, localized inflammation, infiltration by M1 macrophages, compensatory hypertrophy, capillary rarefaction, enhanced levels of TGF- β 1, and myocardial fibrosis. These changes occur in the setting of a systemic pro-inflammatory state that also documents an active process of cardiomyocyte death as per increases in troponin I levels.

The cardioprotective role of estrogen in women is well recognized. However, ~2/3 of HFpEF patients are older women suggesting that as estrogen levels decrease with menopause, they allow for the development of the disease in at-risk patients. Thus, the investigation of the role of estrogens in HFpEF development would require the use of aged female rodents. However, rats and mice do not incur in menopause. Thus, ovariectomy has served as a reliable means for depleting circulating levels of estradiol and assessing its impact on multiple physiological systems. Female HFpEF patients also commonly present with conditions or comorbidities such as hypertension and excess body weight.^{21,22} In this regard, a very limited number of pre-clinical studies have used such models to examine their impact on cardiac fibrosis. In aged ovariectomized rats, we reported on the presence of endocardial and papillary fibrosis suggesting that low estrogen levels can facilitate a greater degree of adverse microstructural remodeling which contribute to the loss of chamber function.⁶

Boluyt *et al.* investigated how aging may affect cardiac structure and function in female F344 rats.²³ Aging female rats demonstrated mild LV dilatation between 13 and 22 months of age. Aging was also associated with increases in collagen content and cross-linking.²⁴ Fannin *et al.* found that increased age in the female F344xBN rat (30 months vs. 6 month) was associated with increases in markers of OS and apoptosis.^{25,26} In young rats, ovariectomy has been reported to cause cardiac structural and functional that include cardiac fibrosis and hypertrophy.²⁷ Ovariectomized rats also exhibit OS and cardiac apoptosis.²⁷⁻³¹ Increases in TNF- α

and IL-1 β are also reported following ovariectomy.^{28–30} Estradiol supplementation of ovariectomized rats reverts increases in apoptosis and cytokines.^{28–31} As reported in our study, ovariectomy allows for hypertension to develop which can aggravate changes in LV structure.³² In hypertensive female rats, ovariectomy can further aggravate myocardial fibrosis and macrophage infiltration, which can be reverted by estradiol treatment.³³ Further evidence for a critical role of estrogens in cardio protection is derived from studies where agonists for the estrogen GPR30 receptor are used as a means to reverse increases in cardiac collagens following ovariectomy.^{34,35} To our knowledge, no studies using aged female rodents have reported on changes in capillary density. However, a recent study of HFpEF patients reported on the presence of LV hypertrophy, fibrosis accompanied by a 27% decreased microvascular density vs. controls.⁸

It is thus, readily apparent that results generated from the use of aged female models of chamber remodeling are very limited with those using ovariectomy as an intervention essentially focused on the use of young animals. Therefore, this is the first study to document the impact that aging-, ovariectomy-, and fructose-induced excess body weight have on LV microstructure and systemic indicators of muscle damage, OS, and inflammation. Pertaining to localized myocardial inflammation (as per inflammatory cell aggregates), aging can trigger notable increases which were further enhanced by ovariectomy suggesting a reliance on estrogen on limiting inflammation and corroborating the reports noted above in ovariectomized young female rodents. The inflammatory infiltrate contained a notable number of macrophages and such changes aligned with increases in circulating levels of GM-CSF, inflammatory cytokines and OS. Of note is that fructose supplemented animals demonstrated further increases in TNF- α and IFN- γ vs. aging alone suggesting that weight gain may aggravate the systemic pro-inflammatory milieu. Cardiomyocyte damage was evident as per increases in blood troponin levels and TUNEL staining. Such changes occurred in the presence of increases in cardiomyocyte surface area and decreases in capillary density. Ultimately, evidence for the participation of the pro-inflammatory cytokine TGF- β 1 in mediating myocardial fibrosis was generated from localized staining and circulating levels which were also further enhanced in fructose-treated animals. It is worth noting that the above describe changes in myocardial microstructure were more evident in endocardium.

In conclusion, we describe our model as pre-HFpEF because in the setting of aging, ovarian hormone depletion and excess body weight (as in the fructose groups) animals demonstrate a significant decrease in CO (Table 1, ~30%) while maintaining a normal EF in the presence of LV fibrosis. However, animals do not appear to demonstrate observable traits of HF such as lack of mobility or feeding. Using this female model of “pre-HFpEF”, notable changes in recognized mediators of tissue remodeling and fibrosis occur which can be aggravated by ovariectomy and excess weight. It is reasonable to speculate that such changes can be further aggravated with time and thus, set the stage for a greater deterioration of LV function. To the extent that these

factors are confirmed in HFpEF patients, they will provide a validation for the use of these animal models so as to further understand underlying pathophysiological processes and evaluate experimental therapies.

Authors' contributions: All authors contributed significantly to conception and design or analysis and interpretation of data and drafting of the manuscript intellectual content.

DECLARATION OF CONFLICTING INTERESTS

The author(s) declared following potential conflicts of interest with respect to the research, authorship, and/or publication of this article: FV is a co-founder of Epirium, Inc. FV and GC are stockholders of Epirium, Inc.

FUNDING

The author(s) disclosed receipt of the following financial support for the research, authorship, and/or publication of this article: Funding was provided by the Department of Defense PR150090, National Institutes of Health DK98717, AG47326 to FV, Consejo Nacional De Ciencia y Tecnologia, Mexico 283938 to IRS, and Apoyo a Proyectos de Investigacion FCS-UP2017 to MLL.

ORCID iDs

Maria L Loredo-Mendoza  <https://orcid.org/0000-0003-2255-1762>

Alejandra Garate-Carrillo  <https://orcid.org/0000-0001-8581-2283>

REFERENCES

- Owan TE, Hodge DO, Herges RM, Jacobsen SJ, Roger VL, Redfield MM. Trends in prevalence and outcome of heart failure with preserved ejection fraction. *N Engl J Med* 2006;**355**:251–9
- Lam CS, Donal E, Kraigher-Krainer E, Vasan RS. Epidemiology and clinical course of heart failure with preserved ejection fraction. *Eur J Heart Fail* 2011;**13**:18–28
- Barandiaran Aizpurua A, Schroen B, van Bilsen M, van Empel V. Targeted HFpEF therapy based on matchmaking of human and animal models. *Am J Physiol Heart Circ Physiol* 2018;**315**:H1670–83
- Omar AM, Bansal M, Sengupta PP. Advances in echocardiographic imaging in heart failure with reduced and preserved ejection fraction. *Circ Res* 2016;**119**:357–74
- Eaton CB, Pettinger M, Rossouw J, Martin LW, Foraker R, Quddus A, Liu S, Wampler NS, Hank Wu WC, Manson JE, Margolis K, Johnson KC, Allison M, Corbie-Smith G, Rosamond W, Breathett K, Klein L. Risk factors for incident hospitalized heart failure with preserved versus reduced ejection fraction in a multiracial cohort of postmenopausal women. *Circ Heart Fail* 2016;**9**:E002883
- Bustamante M, Garate-Carrillo A, BR, Garcia R, Carson N, Ceballos G, Ramirez-Sanchez I, Omens J, Villarreal F. Unmasking of oestrogen-dependent changes in left ventricular structure and function in aged female rats: a potential model for pre-heart failure with preserved ejection fraction. *J Physiol (Lond)* 2019;**597**:1805–17
- King JB, Azadani PN, Suksaranjit P, Bress AP, Witt DM, Han FT, Chelu MG, Silver MA, Biskupiak J, Wilson BD, Morris AK, Kholmovski EG, Marrouche N. Left atrial fibrosis and risk of cerebrovascular and cardiovascular events in patients with atrial fibrillation. *J Am Coll Cardiol* 2017;**70**:1311–21
- Mohammed SF, Hussain S, Mirzoyev SA, Edwards WD, Maleszewski JJ, Redfield MM. Coronary microvascular rarefaction and myocardial

- fibrosis in heart failure with preserved ejection fraction. *Circulation* 2015;**131**:550-9
9. Frangogiannis NG. Cardiac fibrosis: cell biological mechanisms, molecular pathways and therapeutic opportunities. *Mol Aspects Med* 2019;**65**:70-99
 10. Biernacka A, Frangogiannis NG. Aging and cardiac fibrosis. *Aging Dis* 2011;**2**:158-73
 11. Eghbali M, Blumenfeld OO, Seifter S, Buttrick PM, Leinwand LA, Robinson TF, Zern MA, Giambrone MA. Localization of types I, III and IV collagen mRNAs in rat heart cells by in situ hybridization. *J Mol Cell Cardiol* 1989;**21**:103-13
 12. Orlandi A, Francesconi A, Marcellini M, Ferlosio A, Spagnoli LG. Role of ageing and coronary atherosclerosis in the development of cardiac fibrosis in the rabbit. *Cardiovasc Res* 2004;**64**:544-52
 13. Lin J, Lopez EF, Jin Y, Van Remmen H, Bauch T, Han HC, Lindsey ML. Age-related cardiac muscle sarcopenia: Combining experimental and mathematical modeling to identify mechanisms. *Exp Gerontol* 2008;**43**:296-306
 14. Mays PK, Bishop JE, Laurent GJ. Age-related changes in the proportion of types I and III collagen. *Mech Ageing Dev* 1988;**45**:203-12
 15. Kajstura J, Cheng W, Sarangarajan R, Li P, Li B, Nitahara JA, Chapnick S, Reiss K, Olivetti G, Anversa P. Necrotic and apoptotic myocyte cell death in the aging heart of Fischer 344 rats. *Am J Physiol* 1996;**271**:H1215-28
 16. Anversa P, Palackal T, Sonnenblick EH, Olivetti G, Meggs LG, Capasso JM. Myocyte cell loss and myocyte cellular hyperplasia in the hypertrophied aging rat heart. *Circ Res* 1990;**67**:871-85
 17. Moreno-Ulloa A, Nogueira L, Rodriguez A, Barboza J, Hogan MC, Ceballos G, Villarreal F, Ramirez-Sanchez I. Recovery of indicators of mitochondrial biogenesis, oxidative stress, and aging with (-)-epicatechin in senile mice. *J Gerontol A Biol Sci Med Sci* 2015;**70**:1370-8
 18. Villarreal FJ, Dillmann WH. Cardiac hypertrophy-induced changes in mRNA levels for TGF-beta 1, fibronectin, and collagen. *Am J Physiol* 1992;**262**:H1861-6
 19. Michaud M, Balardy L, Moulis G, Gaudin C, Peyrot C, Vellas B, Cesari M, Nourhashemi F. Proinflammatory cytokines, aging, and age-related diseases. *J Am Med Dir Assoc* 2013;**14**:877-82
 20. Goligorsky MS. Microvascular rarefaction: the decline and fall of blood vessels. *Organogenesis* 2010;**6**:1-10
 21. Borlaug BA. The pathophysiology of heart failure with preserved ejection fraction. *Nat Rev Cardiol* 2014;**11**:507-15
 22. Borlaug BA, Paulus WJ. Heart failure with preserved ejection fraction: pathophysiology, diagnosis, and treatment. *Eur Heart J* 2011;**32**:670-9
 23. Boluyt MO, Converso K, Hwang HS, Mikkor A, Russell MW. Echocardiographic assessment of age-associated changes in systolic and diastolic function of the female F344 rat heart. *J Appl Physiol (Physiol)* 2004;**96**:822-8
 24. Thomas DP, Cotter TA, Li X, McCormick RJ, Gosselin LE. Exercise training attenuates aging-associated increases in collagen and collagen crosslinking of the left but not the right ventricle in the rat. *Eur J Appl Physiol* 2001;**85**:164-9
 25. Fannin J, Rice KM, Thulluri S, Dornon L, Arvapalli RK, Wehner P, Blough ER. Age-associated alterations of cardiac structure and function in the female F344xBN rat heart. *Age (Dordr)* 2014;**36**:9684
 26. Fannin J, Rice KM, Thulluri S, Arvapalli RK, Wehner P, Blough ER. The effects of aging on indices of oxidative stress and apoptosis in the female Fischer 344/nnia X brown Norway/BiNia rat heart. *Open Cardiovasc Med J* 2013;**7**:113-21
 27. Lee SD, Kuo WW, Ho YJ, Lin AC, Tsai CH, Wang HF, Kuo CH, Yang AL, Huang CY, Hwang JM. Cardiac fas-dependent and mitochondria-dependent apoptosis in ovariectomized rats. *Maturitas* 2008;**61**:268-77
 28. Stice JP, Chen L, Kim SC, Jung JS, Tran AL, Liu TT, Knowlton AA. 17beta-Estradiol, aging, inflammation, and the stress response in the female heart. *Endocrinology* 2011;**152**:1589-98
 29. Baeza I, Fdez-Tresguerres J, Ariznavarreta C, De la Fuente M. Effects of growth hormone, melatonin, oestrogens and phytoestrogens on the oxidized glutathione (GSSG)/reduced glutathione (GSH) ratio and lipid peroxidation in aged ovariectomized rats. *Biogerontology* 2010;**11**:687-701
 30. Fabris B, Candido R, Bortoletto M, Toffoli B, Bernardi S, Stebel M, Bardelli M, Zentilin L, Giacca M, Carretta R. Stimulation of cardiac apoptosis in ovariectomized hypertensive rats: potential role of the renin-angiotensin system. *J Hypertens* 2011;**29**:273-81
 31. Liou CM, Yang AL, Kuo CH, Tin H, Huang CY, Lee SD. Effects of 17beta-estradiol on cardiac apoptosis in ovariectomized rats. *Cell Biochem Funct* 2010;**28**:521-8
 32. Hinojosa-Laborde C, Craig T, Zheng W, Ji H, Haywood JR, Sandberg K. Ovariectomy augments hypertension in aging female dahl salt-sensitive rats. *Hypertension* 2004;**44**:405-9
 33. Mori T, Kai H, Kajimoto H, Koga M, Kudo H, Takayama N, Yasuoka S, Anegawa T, Kai M, Imaizumi T. Enhanced cardiac inflammation and fibrosis in ovariectomized hypertensive rats: a possible mechanism of diastolic dysfunction in postmenopausal women. *Hypertens Res* 2011;**34**:496-502
 34. Alencar AK, da Silva JS, Lin M, Silva AM, Sun X, Ferrario CM, Cheng C, Sudo RT, Zapata-Sudo G, Wang H, Groban L. Effect of age, estrogen status, and Late-Life GPER activation on cardiac structure and function in the Fischer344xBrown Norway female rat. *J Gerontol A Biol Sci Med Sci* 2017;**72**:152-62
 35. Wang H, Jessup JA, Lin MS, Chagas C, Lindsey SH, Groban L. Activation of GPR30 attenuates diastolic dysfunction and left ventricle remodelling in oophorectomized mRen2.Lewis rats. *Cardiovasc Res* 2012;**94**:96-104

(Received November 5, 2019, Accepted February 17, 2020)